2011

Characterization of Nanofluids with Elongated Nanoparticles

Valentina Baio
Lehigh University

Characterization of Nanofluids with Elongated Nanoparticles

By

Valentina Flavia Baio

A Thesis

Presented to the Graduate and Research Committee

of Lehigh University

in Candidacy for the Degree of

Master of Science

In

Mechanical Engineering

Lehigh University

April 2011

Thesis is accepted and approved in partial fulfillment of the requirements for the Master of Science in Mechanical Engineering

Characterization of Nanofluids with Elongated Nanoparticles
Valentina Flavia Baio

_____

Date Approved

_____

Dr. Sudhakar Neti
Advisor

_____

Dr. Alp Oztekin
Co-Advisor

_____

Dr. Gary Harlow
Department Chair Person

Acknowledgements

I would like to take this time to thank everyone who contributed in any way to this research. Thank you to Dr. Wojciech Misiolek for his help and expertise in attempting to make the alumina nanotubes. Thank you to Dr. Mark Snyder and his lab, Qianying "Bonny" Guo in particular, for their help and guidance during the synthesis of the titania nanoparticles. Thank you to William Mushock for this guidance during the SEM analyses. Thank you to Dr. Raymond Pearson and his lab for the use of their rheometric equipment. Thank you to C-Therm, particularly Adam Harris and Nicole Wooden, for their contribution of the thermal conductivity analyses performed by modified transient plane method. I would like to thank Dr. Satish Mohapatra and Dynalene for the extensive use of the labs and equipment. Thanks to YiJun Yang for being such a great role model and for all his help. Most importantly I would like to thank my advisors, Dr. Sudhakar Neti and Dr. Alp Oztekin, for their help, guidance, and encouragement.

Lastly, I would like to thank my family for their patience, love, and support, and my fiancé Scott for his love and encouragement.

TABLE OF CONTENTS

Page

LIST OF FIGURES

Page

Abstract

Nanofluids have been expected to revolutionize the heat transfer industry by allowing for smaller heat exchangers and using less energy to run equipment. This is ascribed to the potential increases in the surface area related to nanoparticles in the fluid, thermal conductivity and heat transfer coefficient increase of a fluid with nanoparticles. Several of the prior works did not delve into the fact that the viscosity of nanofluids could dramatically be larger. Thus physical property determination is essential for the gainful use of nanofluids, and the present work is an effort toward the determination of the physical properties of a some nanofluids including those with elongated titania nanoparticles in the fluid. Measurement results for particle size, viscosity, and thermal conductivity at various concentrations will be presented and discussed.

Chapter 1. Introduction

Heat transfer concerns the transfer of thermal energy from one physical system to another. Heat transfer is classified into heat conduction, convection, thermal radiation, and phase-change transfer. For our purposes we will be examining only conduction and convection. While conduction happens with both liquids and solids, convection only occurs with liquid fluids. Heat conduction is the exchange of energy of particles such as electrons and phonons in the two systems. When a temperature gradient exists between two objects, heat flows so that the body and the surroundings reach thermal equilibrium by reaching the same temperature. Convection occurs when a flowing fluid carries heat along with the flow of matter in the fluid.

Energy transfer as heat can be improved in one of several ways. Methods for increasing heat transfer include increasing the temperature difference between the object and the environment, increasing the convection heat transfer coefficient, or increasing the surface area of the object. Fins, or any kinds of protrusion, can increase the surface area, thereby increasing the heat transfer. Adding nanoparticles to a fluid would act similarly to fins on a surface of an object. Since nanoparticles usually have a higher thermal conductivity than the base fluid, the addition of nanoparticles to the fluid would already be beneficial. If elongated nanoparticles are added, then there could be the added benefit of a higher surface area. The purpose of this research is to see if this hypothesis is correct. If there is an increase in the thermal conductivity of a fluid when nanoparticles are added, it is necessary to know what other effects the nanoparticles have on the base fluid and if the increase is thermal conductivity can be quantitatively connected to any characteristics of the nanofluid. For example, if as higher concentrations of nanoparticles are added to the fluid, the viscosity increases at the same rate that

the thermal conductivity increases, then the benefits of the increased thermal conductivity will be outweighed by the need for more pumping power due to the increase in viscosity.

In order to characterize nanofluids, tests for the particle size, viscosity, and thermal conductivity are to be done. Particle size is measured by using a Dynamic Light Scattering (DLS) device, which reflects peaks corresponding to the characteristics lengths on hand, sonication and ultrasonic mixing is used to ensure that there is no particle agglomeration and that the particle size distribution is uniform throughout the nanofluid.

The viscosity of the fluid is measured using a concentric cylinder rheometer to check for shear thinning as well as any changes in viscosity due to the nanoparticles added. The thermal conductivity is measured using two different methods: nanoflash and a modified transient plane source technique. The two different methods are used to ensure that the results are consistent and repeatable.

The transient planar source technique works by applying a known current to a sensor's heating element, which results in creating a small amount of heat. This heat input causes a small temperature rise in the sample which in turn causes a change in the voltage of the sensor element. This change in the voltage is used to determine the thermal conductivity based on the transient response as done by C-Therm. Nanoflash works by using a lamp to apply a momentary burst of energy to the bottom of a sample. This causes a small temperature rise in the sample which is detected by an IR detector. This change in temperature is used to determine the thermal conductivity of the sample based on the transient response.

The nanofluid used in the current experiments is composed of distilled water as the base fluid with titania (TiO_2) nanoparticles. The nanoparticles are made in-house and are synthesized

to be of different aspect ratios. Four different aspect ratio tubes are tested, (AR = 1, 4, 7 and 10) to determine the effects of morphology of the nanoparticles on thermal conductivity of the nanofluid. The effect of particle concentration on thermal conductivity is also tested by varying the volume concentration of the nanoparticles.

The subsequent chapters will be arranged as follows: Chapter Two will go over current and past studies that are relevant to our work, Chapter Three will cover the instrumentation used in the present work, Chapter Four covers work done with spherical nanoparticles, which led us to our work with elongated particles, Chapter Five will discuss the nanoparticle selection process, Chapter Six will go over the experimental results and discussion, Chapter Seven will go over the conclusions, and Chapter Eight will discuss future work.

Chapter 2. Literature Review

The study of the effect of nanoparticles on the thermal conductivity of fluids has been an ongoing area of research for many years. The most popular models which predict these effects are the Maxwell model and Hamilton Crosser model, among others. In 1891 Maxwell proposed a model which could be used to predict the thermal conductivity of solid liquid suspensions, although back then nanoparticles did not exist, so the mixtures would have to employ macrosized particles, which would not be practical in flowing systems due to clogging. His model, however, took into account the thermal conductivity of the base fluid, the thermal conductivity of the solid, and the particle volume fraction. Hamilton Crosser is based off of Maxwell's model, but it also takes into consideration the shape factor of the particle, $n=3/\psi$, where ψ is the sphericity of the particle. These models are also all based off of Fourier's law of heat conduction, which states that the heat flux is directly proportional to the temperature gradient. The total energy conducted can be evaluated based on the flow area and temperature difference. A simple one dimensional representation of the Fourier law equation can be seen below, where q is the heat flux, k is the thermal conductivity, and dT/dx is the temperature change across the material. This equation is also what the nanoflash equipment and the transient plane equipment are based on.

According to a study by Choi in [1][2], the Maxwell model and the Hamilton Crosser model do not accurately predict the results of the thermal conductivity of a nanofluid. His research group used multiwall carbon nanotubes dispersed in oil and employed a transient hot wire method to calculate the thermal conductivity of the nanofluid. He found that the results were of one order magnitude greater than the models had originally predicted. These results

seem to be unreasonably large. He also found that there was not a linear relationship between the increase in thermal conductivity and the amount of nanoparticles in the fluid by volume fraction. He speculates this is due to the behavior of the nanoparticles at these large concentrations. In other words, more particles equal more particle to particle interactions. He also believes that the size and shape of the nanoparticle used has a strong influence on the results. He has also done studies on nanofluids with oxide nanoparticles, which is relevant to this work [3]. Since then there has been much speculation by his colleagues at Argonne National Lab that those results were not correct.

Kabelec [4], and Buongiorno [5] who compiled results on aqueous nanofluids from fourteen laboratories, shows that there is also an increase in the thermal conductivity, which correlates to an increase in volume fraction of nanoparticles in water. A variety of different types of nanoparticles were tested in these experiments such as copper, alumina, silica, and even titania. One particular study done by Murshed [6] interests us since he compares the effects of elongated and spherical titania on the thermal conductivity. He found that there is a 2-4% increase between the thermal conductivity of spherical titania and titania nanorod, with the rods always showing a higher thermal conductivity. The results were also about 12% higher than the Hamilton Crosser model and the Maxwell model. Besides studying the effects of types of nanoparticles, some research groups have been studying the effects of base fluids of the thermal conductivity, such as Xie [7].

The research group including Routbort [8] [9], as well as work by Yu [10], Xuan [11], Peterson [12], and Wang [13] has found that the thermal conductivity enhancement is dependent upon particle shape are well as size. They have found that nanorods increase the thermal conductivity more than spherical nanoparticles do, and that this increase in thermal conductivity

also increases as the volume fraction increases. At just 1% vol loading of particles there is a 5% increase in the thermal conductivity. They also suggest that the viscosity of a nanofluid will increase as the concentration of nanoparticles is increased, which will in turn affect the pumping power of the system [14]. The current work includes viscosity measurements of nanofluids to compare the current results to those of others.

One other research group which has shown a very large increase in the thermal conductivity of a fluid by adding nanoparticles is Dispersia Ltd. of England, led by Ding [15]. This group has also done experiments with a variety of nanoparticles, most important to us being the titania particles. They showed that the increase in thermal conductivity compared to the volume fraction follows the modified Hamilton-Crosser model, which can be seen below. The modified version takes into account the effects of shape factor, the thermal conductivity of the nanoparticle aggregates, and the volume fraction. This same group also did rheological experiments on the nanofluids and is one of the few groups to have done such measurements. They suggest that nanofluids with rod-shaped nanoparticles are more likely to be non-Newtonian and exhibit shear thinning.

$$k_{nf}/k_l = \frac{k_a + (n-1)k_l - (n-1)\varphi_a(k_l - k_a)}{k_a + (n-1)k_l + \varphi_a(k_l - k_a)}$$

Other groups to have done rheological experiments include Kwak and Kim [16], Prasher [17], Praveen [18], and Tsai [19].

The results and analysis of the thermal conductivity, viscosity, and particle size of the nanofluids measured here will be presented and discussed in the following chapters.

Chapter 3. Instrumentation

In the present chapter we shall discuss the various instrumentation used for the measurements. Titania particles in the current work were left in the water in which they were synthesized and were thus never dry and needed no mixing. When carbon nanoparticles were used in the present work with oils, mixing was necessary. In order to mix the nanofluids two different tools were used: a sonicator and a homogenizer. The sonicator uses ultrasonic energy to agitate the particles in the fluid and therefore create a homogeneous mixture. The homogenizer uses high speeds to mix the fluid. This mixing process was done at ten minute intervals so that the fluid would not get too hot. The number of intervals which were done depended on the visual stability of the nanofluid. For example, if after four ten minute mixing sessions the nanoparticles were not settling, the fluid was taken to the particle size analyzer. If the nanoparticles settled right away, the fluid was mixed until no settling occurred. If the particle size measurements showed that the particles were still micron size, then the fluid was taken back to be mixed some more.

The particle size of nanofluids was measured using a dynamic light scattering device (DLS) , and where possible also using, wetSEM. DLS uses the principles behind Rayleigh scattering and Brownian motion to measure the average particle size. Rayleigh scattering is the scattering of light by particles much smaller than the wavelength of the light. Brownian motion is used to describe how over time particles in a solution move from areas of high concentration to areas of low concentration, although the method is more random than diffusion. The particles move by means of any outside forces. Using these two principles and the dynamic data collected during the experiment, the average particle size can be found using an autocorrelation of the intensity trace. The limitations associated with the DLS are due to the fact that we are using

elongated particles. The light is reflected off of the particles, but since they are long, it is unknown if what we are measuring is the length or the diameter of the particle, which will throw off the average particle size measurement reading.

WetSEM uses capsules made by Quantomix. The wetSEM method is used to measure the size distribution of particles suspended in a fluid. The wetSEM capsules have a screen on top, and a void in the middle which can be filled with a liquid. This enables a liquid to be viewed in a Scanning Electron Microscope (SEM), which would allow for particle size analysis by actually viewing the particles while still suspended in the liquid. Before the possibility of wetSEM measurements, the nanofluids which were viewed in the SEM had to be dried, which could cause agglomeration and yield incorrect particle sizes. With wetSEM, there is no agglomeration since the nanoparticles are still suspended in the basefluid, resulting in accurate particle size measurements. An image of the wetSEM capsule can be seen in Figure 1 below.

Figure 1: WetSEM Capsules used to view nanoparticles while suspended in fluids

The viscosity of the fluids were measured using an ARES Rheometer with a Couette apparatus. The Couette apparatus has a geometry like two concentric cylinders. An image of this can be seen in Figure 2 below.

Figure 2: Couette Geometry used in the Ares Rheometer

With the Couette geometry, the larger cylinder is filled with the fluid to be tested and the inner cylinder is lowered into this larger one, thus creating a thin space between the walls of the cylinders where the fluid resides. When the experiment begins, the inner cylinder spins at a pre-set speed which is set to increase during the experiment. Since the dimensions of the cylinders and cavities are known and the shear rate is known, using Newton's law of viscosity, $\tau = \mu$, where τ is the shear stress, du/dx is the change in velocity over the thickness of the fluid, and μ is the viscosity, the viscosity can be determined.

The thermal conductivity of the fluid was measured using two methods. The first is the Netzsch nanoflash device and the second is the C-Therm modified transient plane source method. The nanoflash device works by having a lamp pulse light beneath the sample, thereby heating it slightly. This change is temperature is detected by an IR detector. The thermal diffusivity of the liquid is measured by the machine by knowing how long it takes for heat to travel through the liquid and cause a temperature rise on the opposite side. By knowing the specific heat and the density of the fluid, and the measured thermal diffusivity, the thermal

conductivity of the fluid can be calculated using the following equation, where D is the diffusivity, C_p is the specific heat, and ρ is the density.

The modified transient planar source works by using a one-sided, interfacial heat reflectance device that applies a constant current heat source to the sample. During testing, the sample absorbs some of the applied heat, therefore increasing its temperature by about 1-3^{o}C. The rest of the applied heat causes a temperature rise at the sensor interface. By using the rate of temperature increase at the sensor, the thermal conductivity can be measured with the following equation, where Q is the applied heat, A is the cross sectional area, k is the thermal conductivity, and dT/dx is the temperature/thickness gradient.

$$Q = Ak\frac{dT}{dx}$$

Chapter 4. Nanofluids with Spherical Particles

The present chapter descibes work done with near spherical nanoparticles as a prelude to work related to pencil like or elongated nanoparticles. The methods developed and procedures used here were standardized as part of this work for use with all the nanofluids. The spherical nanoparticles were used in convective heat transfer tests to measure their effectiveness. The near spherical particles used were NB50, which are spheres that are 50% diamond and 50% graphite (graphene layer).

These convective heat transfer tests were performed on an annular tube counter flow heat exchanger at Dynalene, Inc. which can be seen in Figure 3 below.

Figure 3: Heat exchanger at Dynalene used for heat transfer tests on spherical nanoparticle nanofluids.

Two Rotameters measured the flow rate of the nanofluid and the chilled water. The flow rate was also measured by removing fluid from the system for about ten seconds, then weighing

the fluid, then dividing the mass of the fluid by the amount of time it was allowed to flow, dm/dt, thereby confirming the Rotameter measurements. Four type T thermocouples were used to measure temperature data at these locations. A PC data acquisition system was used to record the temperature at four different locations: $T_{cold\ in}$, $T_{cold\ out}$, $T_{hot\ in}$, T_{hotout}.

Several base fluids were tried with the nanodiamond (NB50) particles. A Polyalphaolefin 4CPS, (or PAO 4CPS), a hydrocarbon chain fluid was the first tested. The PAO was mixed for twenty-five minutes with 1% by weight of NB50. Only the sonicator was used for this first attempt and by the next day the fluid and the nanodiamond particles had separated. PAO 2CPS was also tried; however, it produced the same results.

Dynalene LO-170 was used next to attempt to make a nanofluid. LO-170 has a flashpoint of 170˚F, which is close to the maximum heater temp at which the system runs; however, since the flow system used is a closed system with no exposure to air/Oxygen, this did not pose as a problem. LO-170 is a branch-chain hydrocarbon with a viscosity of 2.6CPS at room temperature. This base fluid was mixed with 0.3% by weight of NB50 for two hours with both the sonicator and the homogenizer, yet this mixture also separated within the next two days.

The next fluid used as a base fluid was Dynalene SF which has a viscosity of 47.5CPS and is made up of aromatic hydrocarbons. This was mixed with 0.1% by weight of NB50 for three hours with both the sonicator and the homogenizer. This mixture proved to be stable, but since the particle size was measured to be around 700nm, it could not be classified as a nanofluid. The fluid was therefore mixed for another two hours, which did bring the particle size down to about 400nm, but still not enough to bring it to our goal of less than 200nm particle size.

It became apparent that no amount of mixing would bring the particle size down enough to have the mixture be considered a nanofluid and additional mixing and dispersing mechanisms

would be needed to aid in the mixing. To that end, an ester surfactant was introduced into the equation. The surfactant was added to the existing SF mixture in 1% by weight. This surfactant addition plus another few hours of mixing managed to bring the particle size down to 200nm for the Dynalene SF fluid and NB50 nanodiamond particle mixture, which is just enough to be considered a nanofluid.

Another base fluid that was tried to see if better results could be obtained was Dynalene 600, a silicone oil. It was mixed with 0.1% by weight of NB50 and 1% by weight of ester surfactant. The three ingredients were mixed for several hours with both a sonicator and the homogenizer. Once the mixture was stable, the particle size was measured to be about 51nm.

The resultant particle diameter in a stationary fluid colloid could be different than the size in a flowing environment. The flow rate is yet another very important variable for the nanofluid and the experiments considered here. The goal is the use of the nanofluids under turbulent flow conditions, ideally at Reynolds number at or above 10,000. Turbulent flow conditions could be useful for the use of nanoparticles since it could help with the dispersion, mixing and mitigate settling of the higher density particles. The success of such a nanofluid colloid would then be industrially significant.

Since the fluid properties change with the addition of nanoparticles (increase of viscosity) flowmeters calibrated for the base fluid need further calibration with the new nanofluid. In order to accurately determine the flow rate of the fluid, the Rotameter needed to be calibrated for each fluid. The calibration was done manually by timing how long it took a certain amount of fluid to flow through the system and then weighing it. Several points were chosen to take measurements at and these were labeled as point one, two, and three, etc. For plain Dynalene SF fluid, point one corresponded to 13g/s, point two to 25g/s, and point three to 41g/s. When SF mixed with

nanodiamonds was run through the system, since the fluid was so dark, it was impossible to measure the flow corresponding to the same 'marker points'. Thus the flow rates were calibrated according to the corresponding pressure drop between the inlet and outlet. This again had to be adjusted for the change in viscosity. At a pressure difference of 1.1psi the flow rate corresponded to 16g/s, at 1.3psi for flow rate of 21g/s, and at 2.7psi the flow rate is 50g/s. With such flow rates it is not possible to obtain turbulent flow with SF based fluids; so laminar conditions had to be used instead.

The Reynolds number is defined as: $\mathrm{Re} = \frac{\rho u D}{\mu} = \frac{4\dot{m}}{\pi D \mu}$, where ρ is the density of the fluid, u is the fluid velocity, D is the pipe diameter, and μ is the viscosity of the fluid. Since the flow rate $\dot{m}$ is equal to ρ·u·A, the greater the flow rate, or larger diameter, the greater the Reynolds number. Equally important is for the fluid not be too viscous, since a large value of μ would make it difficult to obtain a large Reynolds number. As mentioned earlier, the viscosity of nanofluids even with relatively small loadings (1% by mass) can be significantly larger than the base fluid. Additionally, the resulting colloidal nanofluid could very well be non-Newtonian with shear thinning properties. Thus care should be taken in evaluating the gains in heat transfer (Nusselt number) as a function of Reynolds number since the increase in Nusselt number can appear to happen at a lower Reynolds number with all other conditions remaining the same.

Once the flow, pressure drop and heat transfer data had been collected, calculations could be done to calculate the heat transfer and the overall heat transfer coefficient. At the time when these experiments were done, the measurements for the thermal conductivity were not well established. The increase in thermal conductivity was assumed to be about 10% above the base

fluid for the heat transfer calculations. Ten percent was chosen because it was a reasonable increase for a loading of 0.1% by mass of NB50 mixture.

After collecting many sets of data, a thorough analysis was done using the log-mean-temperature difference (LMTD) method for the double pipe apparatus. It was found that for plain SF fluid and SF +.1% NB50 fluid, the flow could only reach laminar conditions even at the highest flow rates. Data was taken at two flow rates: point "1" which was 0.013kg/s, and point "two" which was 0.025kg/s. Using the equations appropriate for the LMTD method, it was found that plain SF produced a heat transfer of 436W and an overall heat transfer coefficient of 11.9 W/m²-K at the lower 0.013 kg/s flowrate (point 1). The nanofluid laminar flow at this same flow rate produced a heat transfer coefficient of 13 W/m²-K and a heat transfer of 468.0W. If the assumption about the thermal conductivity is correct, a .013kg/s there is an increase of 6.8% for the heat transfer.

At a flow rate of 0.025 kg/s, plain SF had an overall heat transfer coefficient of 11.9 W/kg*m² and a total heat transfer of 445.8 W. The nanofluid had an overall heat transfer coefficient of 13W/m²-K and a heat transfer of 550.0W. Assuming again an increase in thermal conductivity of 10% for the nanofluid, this means that at .025kg/s, there is an increase of 18.9% in the heat transfer. Since these tests were done, we have found that the assumed 10% increase in the thermal conductivity could be an overestimation of the increase in thermal conductivity for the nanofluid, especially for the spherical nanoparticles. With the expectation that elongated particles could do better with various desired properties, production and the characterization of the nanofluids was done. The next chapters deal with efforts to generate Al_2O_3 and elongated Titania particles and the determination of the properties.

Chapter 5. Nanoparticle Selection

Since most of the previous research had been done on spherical nanoparticles, the present work focuses on elongated particles dispersed into either aqueous or organic base fluids. One type of nanoparticle considered here was alumina (Al_2O_3). Since it was not possible to make elongated Al_2O_3 nanoparticles in house to the specifications that were desired, nanosized alumina membrane discs were purchased from Whatman. The membrane discs are used as filters, which meant that they were essentially clusters on alumina nanotubes. Two different pore sizes were ordered, the 20nm and the 200nm. A scanning electron microscopy (SEM) image of the 200nm disc can be seen in Figure 4. The 20nm disc looks the same except the pores are smaller. The discs were 13mm in diameter and 60μm thick.

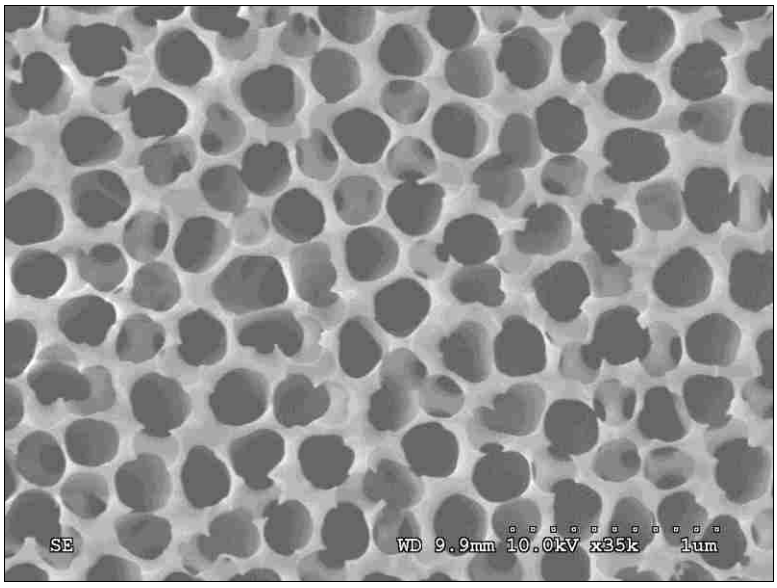

Figure 4: SEM image of 200nm Alumina Disc from Whatman

In order to separate the membranes into individual tubes which could then be dispersed into a base fluid, the discs had to be processed. Two different methods were tried in order to break the membranes without destroying the tube structure. The first method was quenching. First the discs were heated to 250C, and then placed into a container full of liquid nitrogen. With

this drastic change in temperature, we hoped the discs would break along the walls, thus providing us with individual tubes. The result was that nothing happened. Next the temperature was raised to 500C, with again the same results. Lastly the temperature was raised to 800C. The result was that the discs curved up into a tube-like shape, thus changing their crystalline property.

Since quenching was unsuccessful, the next attempt made to break up the membranes was to put them in Retsch planetary ball mills. In order to successfully determine the proper milling procedure to obtain individual alumina nanotubes from a honeycomb membrane disc, several experiments had to be done. The milling parameters which act as the variables are the rotational speed, the amount of grinding balls, the material of the grinding balls, the amount of alumina discs used, and pore size of the alumina. In order to determine which variable has the most significant effect on the end result, only one variable was changed at a time. The goal was not only to obtain individual nanotubes, but also retain the high aspect ratio of the tubes.

On the first visit to Retsch, five samples were tested in the grinding experiments. For our purposes we will call them samples 1A, 2A, 3A, 4A, and 5A. A 12mL jar made of stainless steel was used to hold all of the materials during the milling procedure. Sample 1A consisted of five discs of 20nm porosity with thirty 5mm stainless steel grinding balls. This sample was milled for five minutes at 400rpm. The results can be seen in Figure 5.

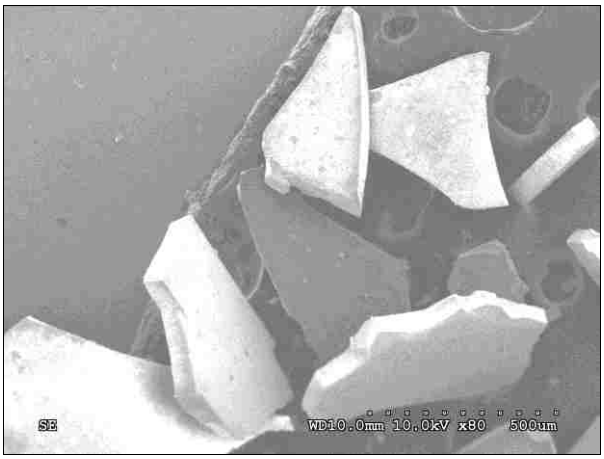

Figure 5: Sample 1A. Results of five discs of 20nm porosity with thirty 5mm stainless steel grinding balls milled for five minutes at 400rpm using the planetary ball mill.

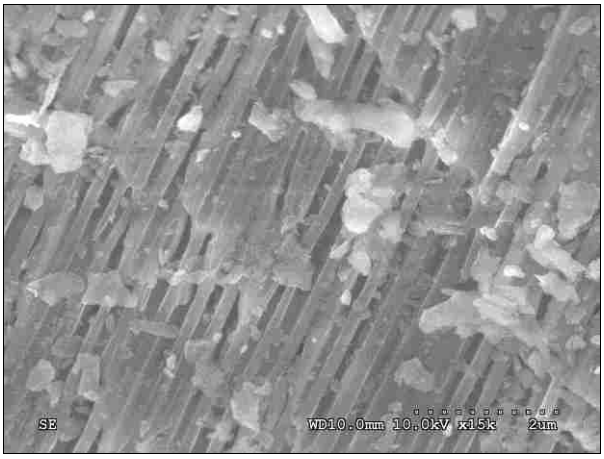

Figure 6: Sample 1A. Results of five discs of 20nm porosity with thirty 5mm stainless steel grinding balls milled for five minutes at 400rpm using the planetary ball mill.

As can be seen in Figure 5, the average particle size distribution is approximately 500µm, which is too large for our application. However, on the positive side, it can be seen that the length of the tubes is intact meaning the discs were not sheared. During the SEM analysis it was also found that there are no contaminants in any of the samples, so the stainless steel from the jar and from the grinding balls did not break down and mix with the alumina.

Sample 2A consisted of ten discs of 200nm porosity with thirty 5mm grinding balls. This sample was milled for five minutes at 400rpm. These results can be seen in Figure 7 and Figure 8. As can be seen, by changing the number of discs from five to ten the particle size distribution

has gone down significantly. The average size of the particles ranges from 20µm to 30µm. Through these parameters some individual tubes were obtained, which can be seen in Figure 8. The original length of these tubes was 60µm, and after milling the alumina, the individual tubes range in length from 2.5µm to about 4µm, making the aspect ratio range from 12 to 20. A higher aspect ratio is desired, meaning the RPM during the milling procedure should be lowered to avoid shearing of the material.

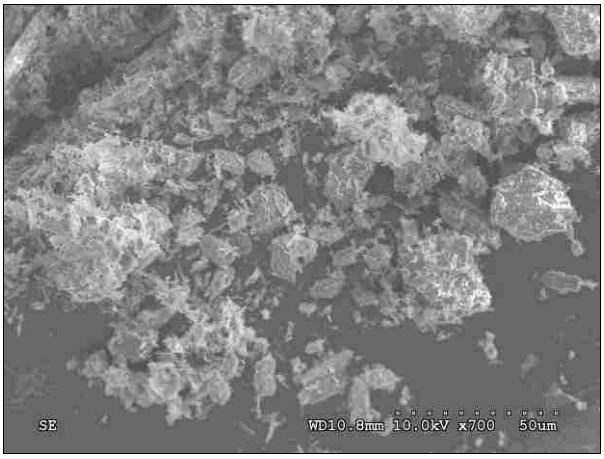

Figure 7: Sample 2A. Results for ten discs of 200nm porosity with thirty 5mm grinding balls milled for five minutes at 400rpm using the planetary ball mill.

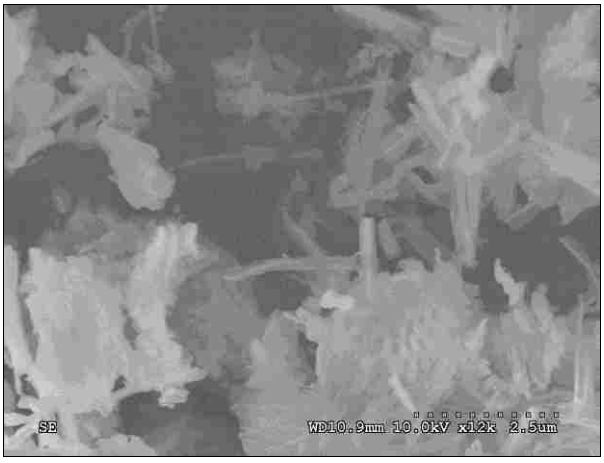

Figure 8: Sample 2A. Results for ten discs of 200nm porosity with thirty 5mm grinding balls milled for five minutes at 400rpm using the planetary ball mill.

Sample 3A consists of ten discs of 200nm porosity with thirty 5mm grinding balls. This sample was milled for five minutes at 300rpm. The results can be seen in Figures 9 and 10.

From Figure 9 it can be seen that the average particle size has gone up to about 60µm. This must be due to the lowering of the milling speed. It can also be seen that some small clusters of about 2µm have a length of about 20µm, so although the aspect ratio is still about ten; the longer length shows that the material is not shearing as much. Figure 10 depicts some individual tubes that were obtained from this procedure. The length of these individual tubes is about 8µm, making the aspect ratio about 40, a large improvement from before.

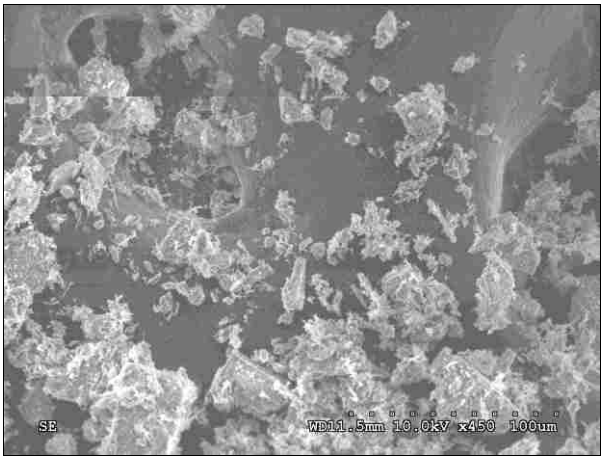

Figure 9: Sample 3A. Results for ten discs of 200nm porosity with thirty 5mm grinding balls milled for five minutes at 300rpm using the planetary ball mill.

Figure 10: Sample 3A. Results for ten discs of 200nm porosity with thirty 5mm grinding balls milled for five minutes at 300rpm using the planetary ball mill.

Sample 4A consists of ten discs of 200µm porosity with only fifteen 5mm grinding balls. This sample was milled for five minutes at 300rpm. The results can be seen in Figures 11 and 12. From Figure 11 it can be seen that the average particle size is 40µm. Compared to sample three which has large particles (~70µm) with a scattering of smaller particles (~50µm), sample four generally has a smaller particles (~25µm), with scatterings of large particles (~75µm). Although the particle size is heading in the right direction, images of the individual tubes that are produced show that the tubes are splintering and not retaining their circular shape. This may be caused by a milling rate that is too high.

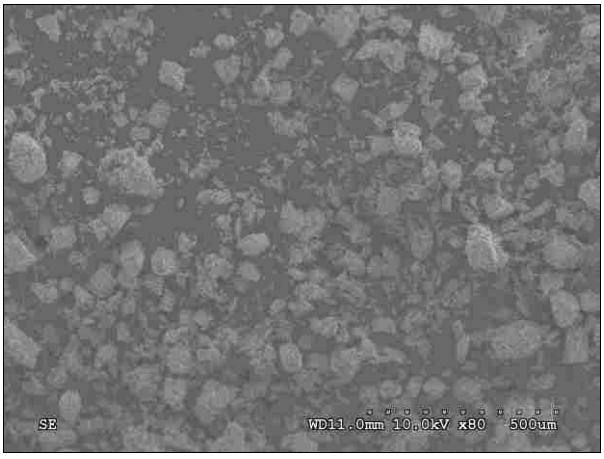

Figure 11: Sample 4A. Results for ten discs of 200µm porosity with only fifteen 5mm grinding balls milled for five minutes at 300rpm using the planetary ball mill.

Figure 12: Sample 4A. Results for ten discs of 200µm porosity with only fifteen 5mm grinding balls milled for five minutes at 300rpm using the planetary ball mill.

Sample 5A consists of ten discs of 200µm porosity with fifteen 5mm grinding balls. These were milled at 300rpm for eight minutes. The results can be seen in Figures 11 and 12. The only difference between sample 4A and sample 5A is the amount of time they were milled. The thinking behind this was that the particle size would become smaller, but as can be seen in Figure 11, this is not the case. In fact it would appear that the average sample size is actually larger, somewhere around 100µm. Also, it would appear from Figure 12 that the individual tubes are splintering even more and are getting sheared more, making the tubes shorter.

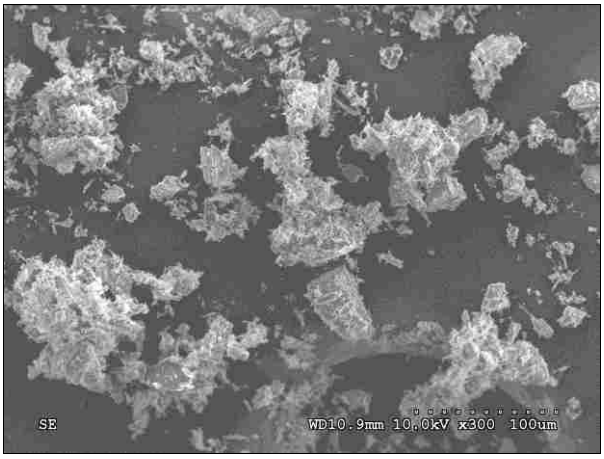

Figure 13: Sample 5A. Results for ten discs of 200µm porosity with fifteen 5mm grinding balls milled at 300rpm for eight minutes using the planetary ball mill.

Figure 14: Sample 5A. Results for ten discs of 200µm porosity with fifteen 5mm grinding balls milled at 300rpm for eight minutes using the planetary ball mill.

After having collected and analyzed the results, sample 4A is the closest one to reaching our goal of having either individual tubes or small clusters of tubes, and still retaining a large aspect ratio. It is apparent that more milling time is not the right direction to go in to obtain more optimal results, so therefore more milling experiments had to be done to find the proper milling parameters.

Further attempts at finding the correct parameters to obtain nano-sized particles were made. A 12mL stainless steel jar was again used for all of the experiments. The main variables that were planned on experimenting with were the grinding speed and the grinding ball material. The length of time for the experiments was also varied. These samples are referred to as 1B, 2B, 3B, 4B, 5B, 6B, 7B, 8B, 9B, 10B, and 11B.

Sample 1B consisted of ten discs of 20nm porosity with fifteen 5mm agate grinding balls. Agate has a density of 2.65g/cm^3. This sample was put into the planetary ball mill for five minutes at 300rmp. At the end of the experiment the discs were mostly unbroken. The agate grinding balls were assumed to be too light, so for the second sample zirconia grinding balls which have a density of about 5.9g/cm^3 were employed.

Sample 2B consisted of ten discs of 20nm porosity with thirty 3mm zirconia grinding balls, since the 5mm grinding balls were not available. This sample was milled for five minutes at 300rpm in the planetary ball mill. Again, nothing happened to this sample, the discs remained mostly unbroken.

Sample 3B consisted of ten discs of 20nm porosity with thirty 3mm zirconia grinding balls. This sample was milled for five minutes at 400rpm in the planetary ball mill. Again the discs remained mostly unbroken. At this point we assume the discs are not seeing enough

impact from the grinding balls, so we must either increase the amount of grinding balls or the speed at which the sample is being milled.

Sample 4B consisted of ten discs of 20nm porosity and forty-five 3mm zirconia grinding balls, so for this sample we increased the amount of grinding balls. This sample was milled for five minutes at 400rpm. The results again showed mostly whole discs.

Sample 5B consists of ten discs of 20nm and forty-five 3mm zirconia grinding balls. This sample was milled for five minutes at 600rpm. Even at such a high speed, the force generated was not enough to break apart the discs.

Since the first five samples from the second set of attempts did not break apart, even when high milling speeds were used, it was apparent that using the zirconia grinding balls in the planetary ball mill was not going to produce satisfactory results. Therefore, when selecting the parameters for sample 6B, stainless steel grinding balls were chosen. Sample 6B consisted of ten discs of 20nm porosity with fifteen 5mm stainless steel grinding balls. The sample was milled for five minutes at 25rpm on the planetary ball mill. The discs were still mostly unbroken.

For sample 7B a different machine that would use more impact force was employed. The machine that was chosen was the Mixer Mill 400, which essentially shakes a canister back and forth at a set frequency. The sample consisted of ten discs of 20nm porosity and forty-five 3mm zirconia grinding balls. It was milled at 25Hz for thirty seconds. The experiment produced results that were worth analyzing in the SEM. After analyzing this sample, it was found that is has an average particle size 166.2μm, as seen in the Figure 15.

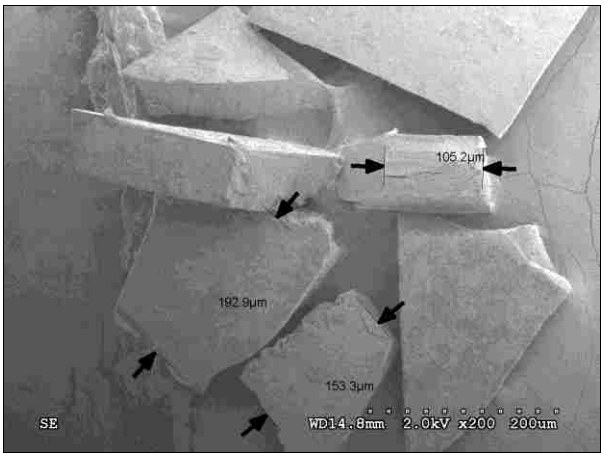

Figure 15: Sample 7B. Results for ten discs of 20nm porosity and forty-five 3mm zirconia grinding balls milled at 25Hz for thirty seconds using the Mixer Mill.

Sample 8B consisted of ten discs of 20nm porosity and forty-five 3mm zirconia grinding balls. It was milled at 25Hz for one minute. After analyzing the sample in the SEM, the average particle size was found to be 498.9µm as can be seen in Figure 16.

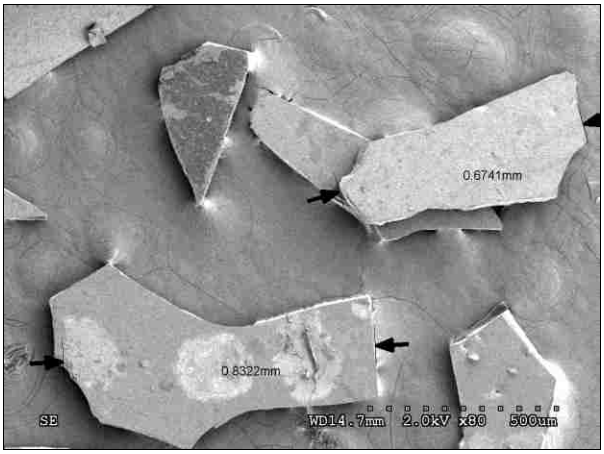

Figure 16: Sample 8B. Results for ten discs of 20nm porosity and forty-five 3mm zirconia grinding balls milled at 25Hz for one minute using the Mixer Mill.

Sample 9B consisted of ten 20nm porosity discs with thirty 5mm stainless steel grinding balls. The planetary ball mill was used at 400rpm for five minutes. After analyzing the sample in the SEM, it was found that the average particle size is 224.2µm. as can be seen in Figure 17.

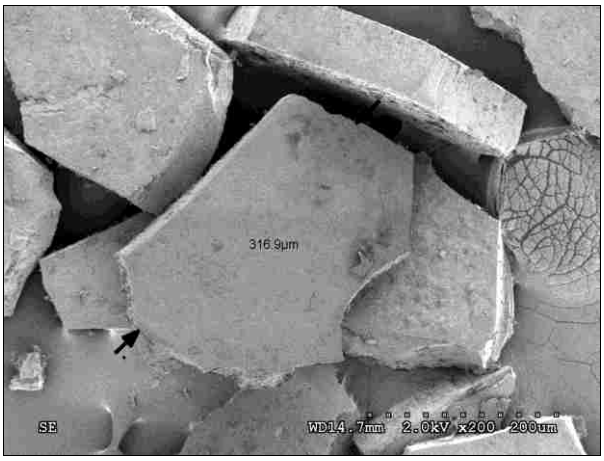

Figure 17: Sample 9B. Results for ten 20nm porosity discs with thirty 5mm stainless steel grinding balls milled at 400rpm for five minutes using the planetary ball mill.

Sample 10B consisted of ten 200nm porosity discs with fifteen 5mm stainless steel grinding balls. The planetary ball mill was used at 300rpm for ten minutes. SEM analysis displays that the average particle size is 72.93µm as can be seen in Figure 18.

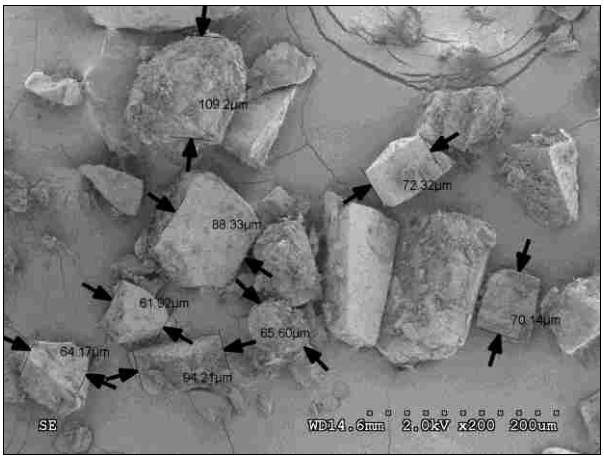

Figure 18: Sample 10B. Results for ten 200nm porosity discs with fifteen 5mm stainless steel grinding balls milled at 300rpm for ten minutes using the planetary ball mill.

Sample 11B consisted of ten 20nm porosity discs with forty-five 3mm zirconia grinding balls. The Mixer Mill (MM400) was used at 25Hz for two minutes. SEM images depict that the average particle size is 310.9µm. The results can be seen in Figure 19.

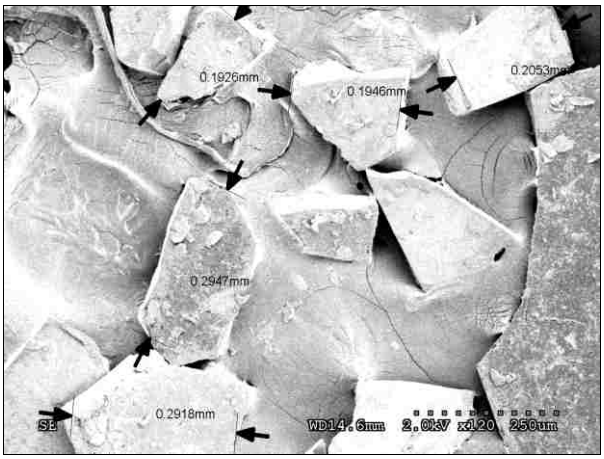

Figure 19: Sample 11B. Results for ten 20nm porosity discs with forty-five 3mm zirconia grinding balls milled at 25Hz for two minutes using the Mixer Mill.

Sample 12B consisted of ten 200nm porosity discs with fifteen 5mm stainless steel grinding balls. The planetary ball mill was used at 250rpm for five minutes. After SEM analysis it was found that the average particle size is 132.2µm. Even though these are the same milling parameters used in sample 6A, the fact that the material to be milled was changed produced completely different results. This may mean that the 20nm porosity discs and the 200µm porosity discs react differently under the same manufacturing conditions; however, this requires further investigation. The results for sample twelve can be seen in Figure 20.

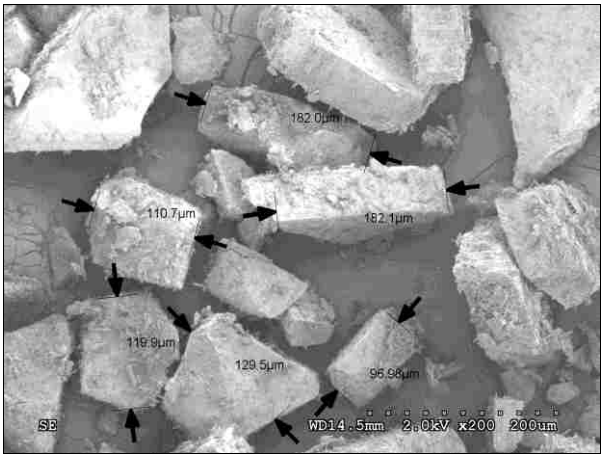

Figure 20: Sample 12B. Results for ten 200nm porosity discs with fifteen 5mm stainless steel grinding balls milled at 250rpm for five minutes using the planetary ball mill.

After close examination of the results, it appears that the Mixer Mill 400 will not give us nano scaled particles. Even when extending the time, the particle size does not decrease sufficiently to promise better results. The results obtained from the planetary ball mill would lead us to believe that the 20nm discs and the 200nm discs do not produce comparable results when milled under the same conditions. Further experimentation is required to prove this. The results obtained when using the planetary ball mill at 250rpm seemed promising, since the material is not smashed as much but only broken apart; however, they are still not the nanoparticles that we had hoped to use in our nanofluid characterization experiments.

When comparing the results for sample 9B, which was the same conditions as sample 1A, it would seem that the results are consistent; however, when comparing sample 10B to sample 5A, the results are inconsistent. The average particle size for sample 10B, which was milled at 300rpm for ten minutes, is about 73µm. The average particle size for sample 5A is about 34µm. These results do not make sense since, even with all other parameters kept the same, as the length of milling time was extended the particle size should decrease. Because this is not the case, we have to assume that the planetary ball mill cannot produce consistent results. A different type of nanoparticle must be sought.

The next attempt at nanoparticles was purchasing multiwall carbon nanotubes and carbon nanofibers. The nanotubes were purchased from SES Research and were 10nm in diameter. An image of them can be seen in Figure 21. As can be seen, these nanotubes are not straight but actually form cluster-like networks that have an average particle size of 150µm, which is very large for our purposes. The carbon nanofibers were purchased from Pyrograph Products and have an average diameter of about 100nm. The average partcicle size of the carbon nanofibers is 250µm, which is even larger than that of the carbon nanotubes. The reason for trying these

cluster-like nanoparticles is that they would form a network in the fluid and therefore would transfer heat more efficiently. Images of these nanofibers can be seen in Figure 22. Neither type of nanoparticle was picked for the project since they were extremely hydrophobic, and would only mix in oils. The equipment available for measuring thermal conductivity does not measure the thermal conductivity of oils accurately; therefore, these nanoparticles were not a suitable choice.

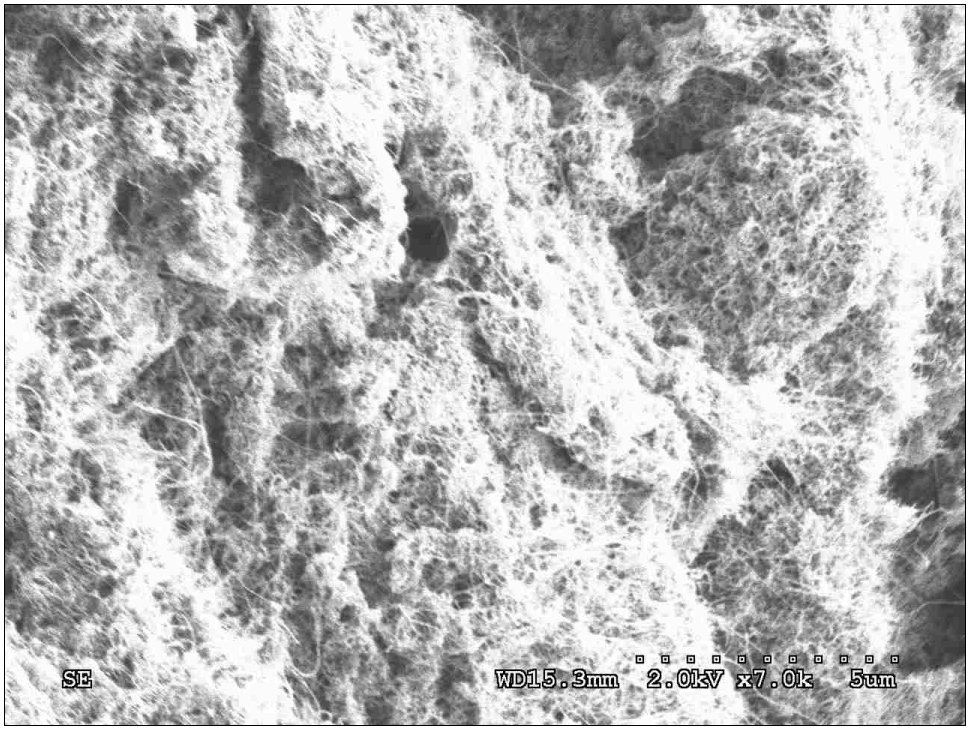

Figure 21: SEM Image of Carbon Nanotubes

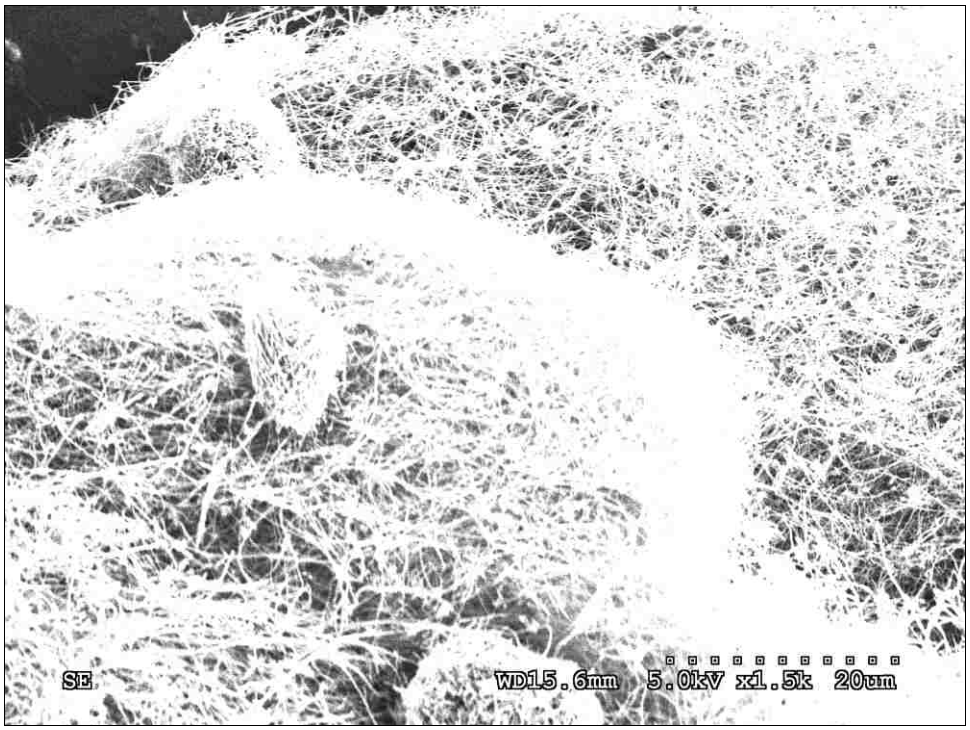

Figure 22: SEM Image of Carbon Nanofibers

The last type of nanoparticle that was tried was titania nanorods. These rods were made in house using the formula described by Zhang and Gao [20]. The first step is to make a 3M solution of $TiCl_4$ in water. To do this, the appropriate amount of water is measured out, then, while stirring, the pre-calculated amount of $TiCl_4$ is added drop by drop to the water. To determine the amount of water and $TiCl_4$ to use, the following equation is used, where $mass_1$ is the amount of $TiCl_4$ in grams, mol_1 is the molecular weight of $TiCl_4$, ρ_1 is the density of $TiCl_4$, $mass_2$ is the amount of water in grams, and ρ_2 is the density of water. It is best to pick an amount of $TiCl_4$ to use and solve for the amount of water.

$$\frac{\frac{Mass_1}{mol_1}}{\frac{Mass_1}{\rho_1}+\frac{Mass_2}{\rho_2}} = 3mol/L$$

Once this stock solution is made, it can be added, again while stirring, drop by drop to more water. Since four different length nanorods were made, the amount of water added to the stock depended on the length of nanorod desired. Generally speaking, the more $TiCl_4$ present in the final solution, the larger the aspect ratio of the nanorod. For this project, aspect ratios of ten, seven, four, and one were used, and the final solutions were 1mol/L, 0.5mol/L, 0.3mol/L, and 0.1mol/L respectively. The reason for using a maximum of ten as an aspect ratio is because the method of synthesis currently available to us only permits a maximum of ten to form. If higher aspect ratios are desired a new method must be found, such as using nanoscale mold in which to grow the titania nanorods. The final step consisted of placing the solutions in autoclaves and letting them sit in furnaces at 453K for twelve hours. After the twelve hours, the titania/water mixtures were removed from the autoclaves. Images of the four types of titania nanoparticles can be seen in Figures 23, 24, 25, and 26.

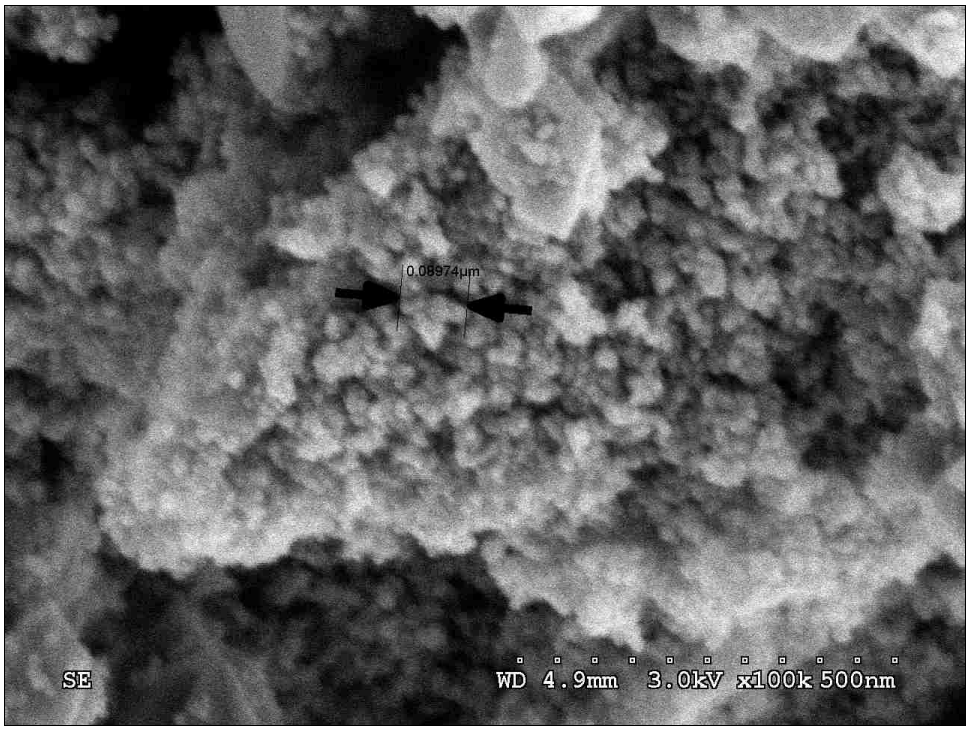

Figure 23: Spherical Titania Nanoparticles

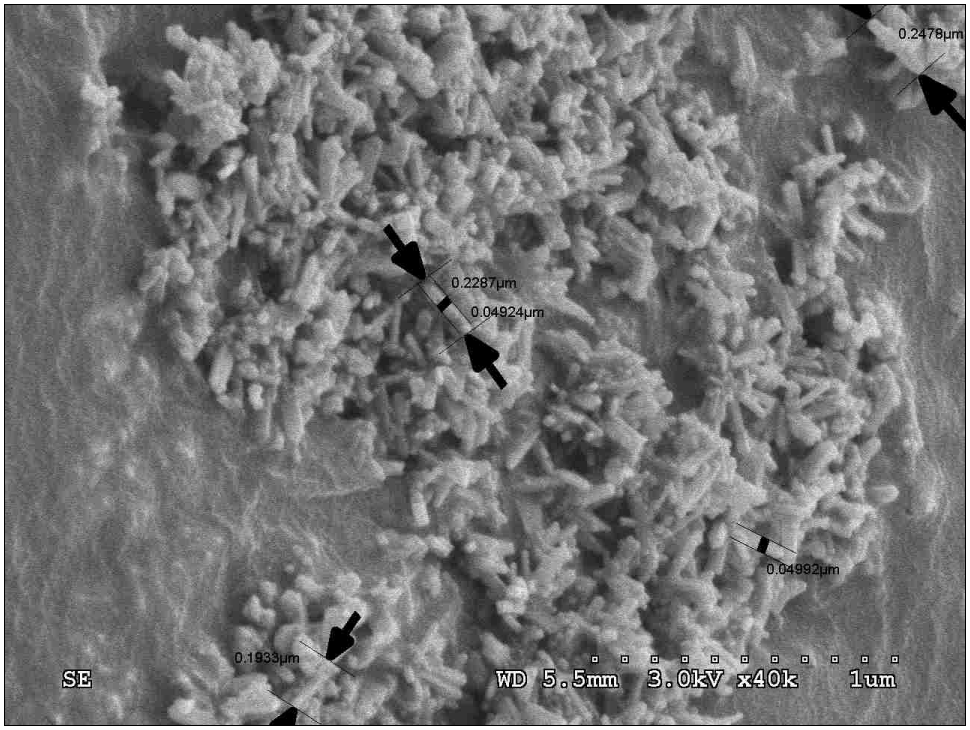

Figure 24: Titania Nanorod of Aspect Ratio Four

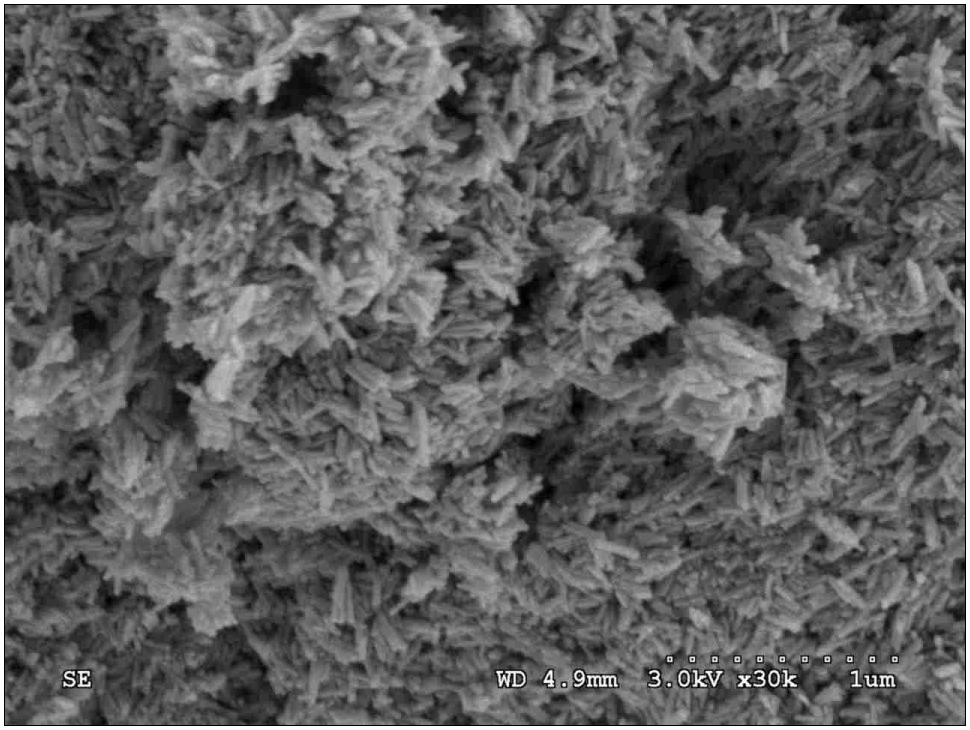

Figure 25: Titani Nanorods of Aspect Ratio Seven

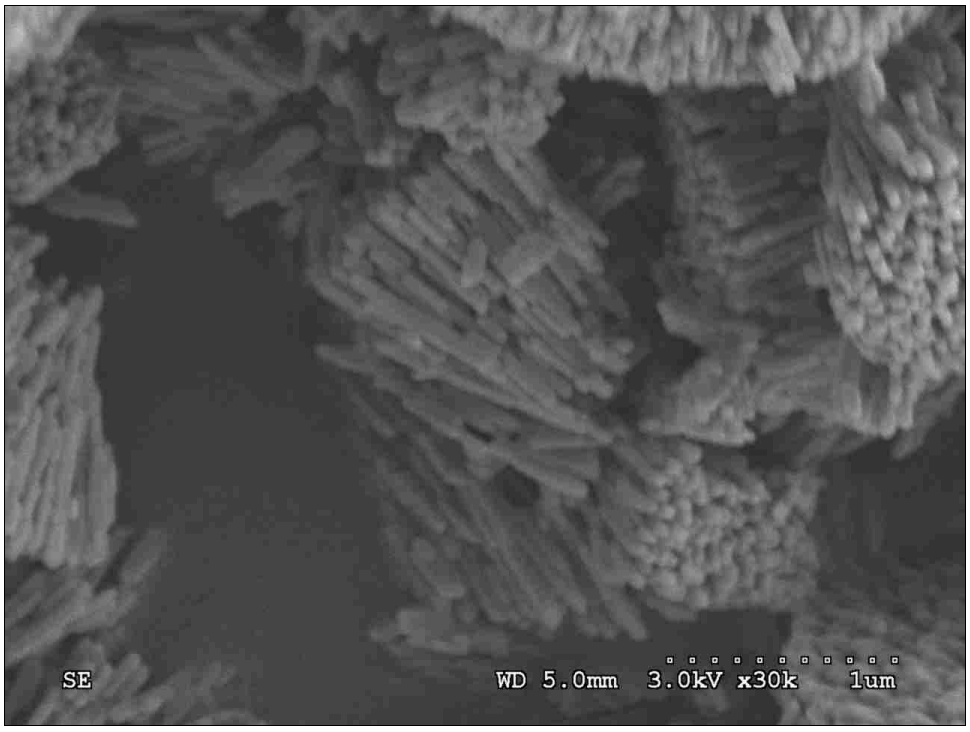

Figure 26: Titania Nanorods of Aspect Ratio Ten

A small sample, about 2-3g, was removed from each type of nanofluid. This sample is used to determine the weight percentage of titania in each type of nanofluid. The liquid form is weighed, then allowed to dry and weighed again. By dividing the weight of the dry by the weight of the wet, the weight percentage can be determined. Depending on whether the concentration is too high or too low, water is added, or removed by centrifuge. At this point, a successful, stable nanofluid has been created, and experiments can be started. One down side to this method of making titania nanoparticles is that it is very limited in the quantities that can be made. Only a maximum of 50ml at 5%wt of each type of nanofluid was able to be made to perform all of the tests. Lower concentrations were not as much of a problem, but if a large enough quantity to run a heat exchanger was needed, it would be extremely unpractical to employ this method of synthesis.

Chapter 6. Experimental Results and Discussion

Carbon nanofibers (CNF) were mixed into two different types of oils, polyalphaolefin (PAO) and syltherm 800. Carbon nanotubes (CNT) were only mixed into Syltherm 800. The particles were added to the base fluids and sonicated for an hour, ten minutes at a time, and were mixed up to a concentration of 8%wt for the PAO and CNF and Syltherm and CNT. The Syltherm and CNF were mixed to a concentration of 1%wt.

The particle size measurements show that all three of these nanofluids are unstable colloids. However, thermal conductivity measurements were performed nonetheless. The particle measurements can be seen in Figure 27. It can be seen that at concentrations exceeding 1%wt, the particle size becomes huge, with a minimum of 704nm using Syltherm and CNT and a maximum of 2179 using PAO and CNF.

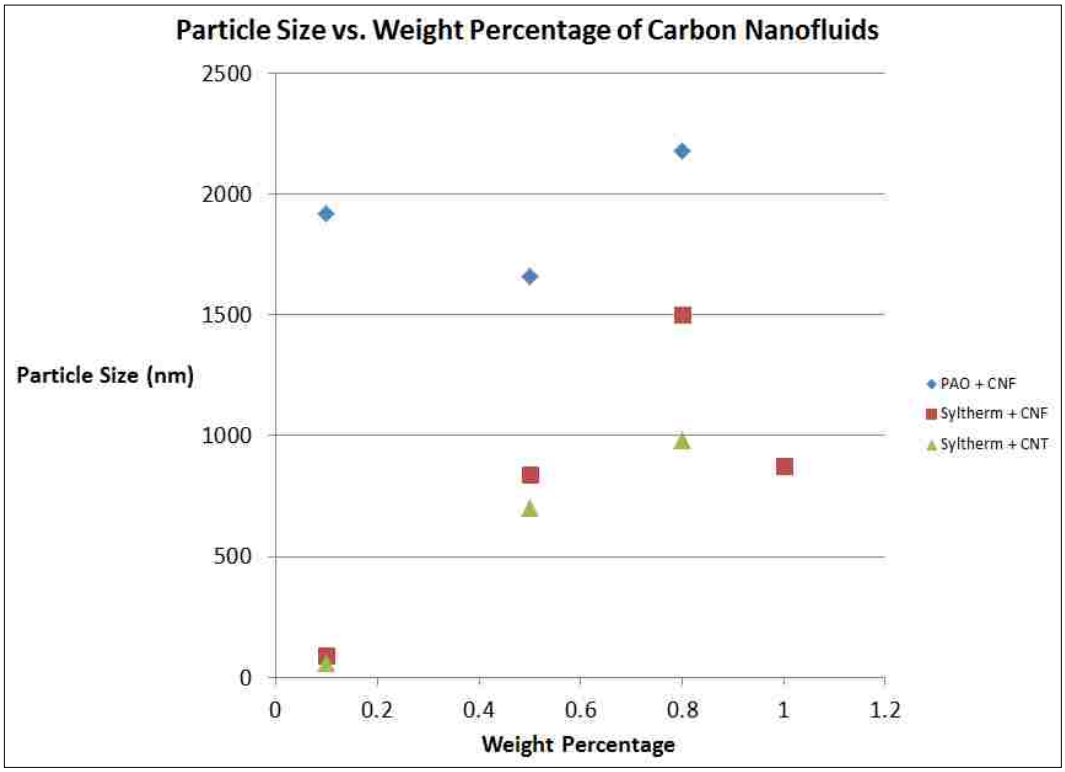

Figure 27: Particle Size measurements of carbon nanofluids vs. weight percentage

Considering these are fairly low concentrations, the fact that these numbers are so high and the particles settle down immediately is cause for concern. They are extremely unstable nanofluids and cannot even really be called nanofluids since the particle sizes are outside the nanoscale range.

The thermal conductivity measurements were taken up to concentrations of 0.8%wt for all three nanofluids. The sample preparation for the nanoflash device is complex and takes some practice. First, a layer of graphite had to be sprayed on, and in order for consistent results to be possible, the graphite had to be applied the same way each time. This mean the same person has to run the tests in order for them to be comparable. In order to place the nanofluid in the machine, a bubble had to be formed in the sample holder. This had to be done by applying a certain amount in the bottom of the holder and then hang a drop of a certain amount of fluid from the cap of the sample holder. Once the cap was put on, the hanging drop and the drop already present in the bottom of the holder would join and create one bubble. If the surface tension was broken, the sample had to be reprepared.

The results for the thermal conductivity measurements can be seen in Figure 28. As can be seen, they are very disappointing. The only increase recorded is when PAO and CNF were used, which shows about a 14% increase in thermal conductivity. This is surprising since CNT have a thermal conductivity of about 3000W/m-K vs CNF which only have a thermal conductivity of 300W/m-K. Even so, the data with the CNT shows absolutely no increase, in fact it would seem there is a slight decrease in the thermal conductivity compared to the plain base fluid. When discussing these results, it was thought that the surface tension of the oil is not high enough to maintain the necessary bubble shape, which would continuously skew the results. Since this problem kept interfering with our measurements, the carbon nanofluids were set aside

until a more stable fluid could be made and a more suitable method of measuring the thermal conductivity could be found.

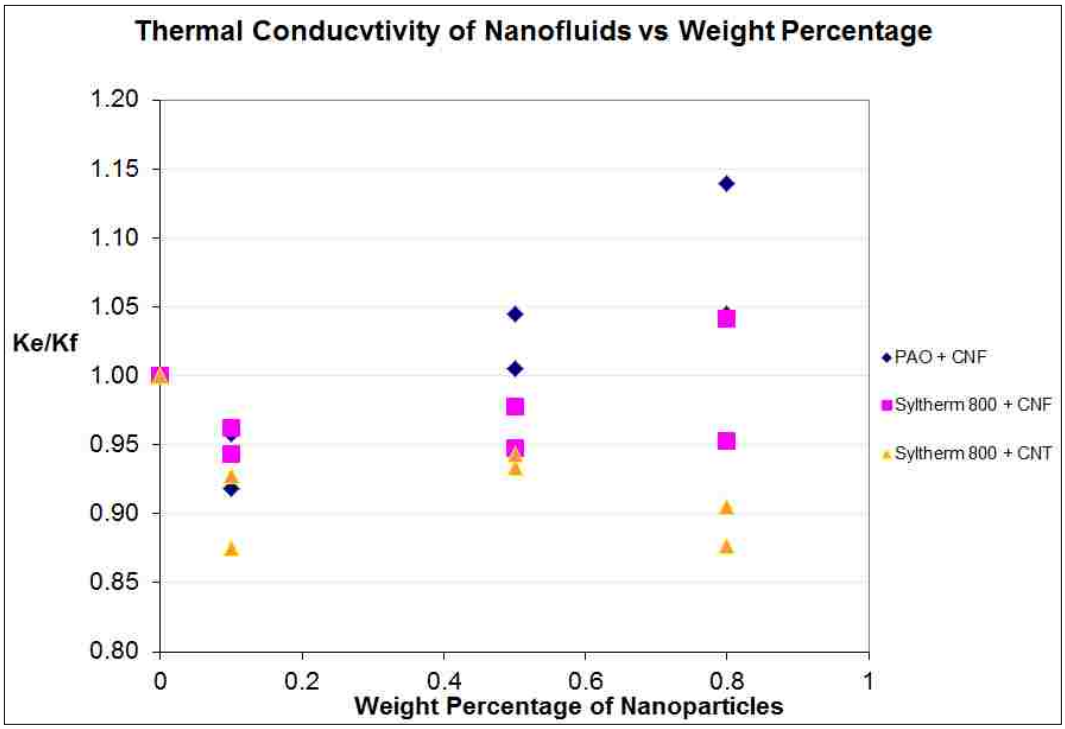

Figure 28: Thermal conductivity of carbon nanofluids vs. weight percentage.

The results for the titania nanofluids proved to be much more promising. The particle size analysis were very interesting. Particle size measurements were taken at 0.1%wt, 0.5%wt, 1%wt, 2.5%wt, and 5%wt. Where elongated nanoparticles were used, two peaks appeared in all of the tests. The two peaks represent the diameter of the rods and the length of the rods. Generally, if the larger peak value is divided by the smaller one, the result is aspect ratio of the nanoparticle. Figure 29 shows a chart of the average particle size for each concentration. As can be seen, the particle size does not follow any particular trend, only that the spherical nanoparticle fluid tends to have the smallest particle size. WetSEM analysis to confirm the DLS data was not

possible with this nanofluid because the nanoparticles were not visible below the surface of the capsule. The material must be of a certain composition in order to show up. For example, when Syltherm 800 with nanodiamonds was tested, the particles showed up right away on the surface. Alumina nanoparticles also seemed to work well, which is why titania was also tried, to no avail however.

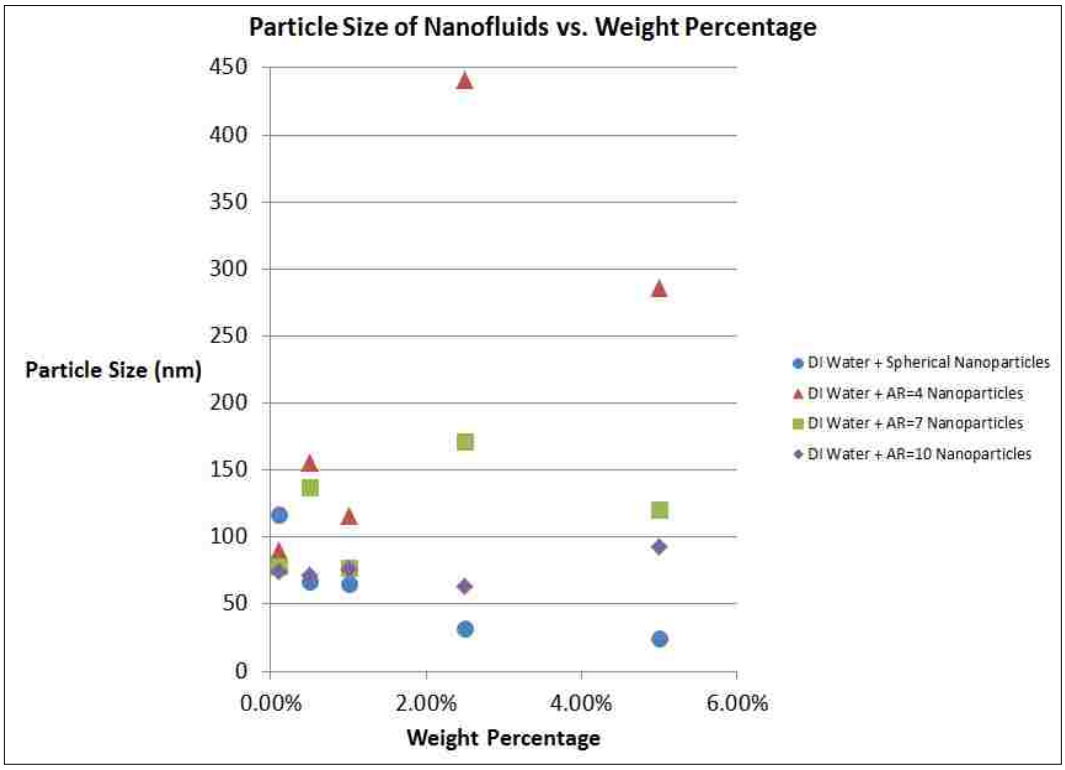

Figure 29: Particle size of titania nanofluid vs. weight percentage.

For titania nanofluid the particle size does not vary considerably as the concentration of particles is increased, as shown in Figure 29. For example, in the case of the nanofluid using particle with an aspect ratio of ten, for all concentrations the particle size stays between 60nm and 95nm. For the nanofluids with particles of aspect ratio one and seven, the particle sizes stay within a 100nm range. The only nanofluid which does not stay within the 100nm range is the one which uses particles of aspect ratio four. This is very strange as the nanofluid was made

exactly the same way as the others and has been handled and stored the same way. Since the particle sizes for this type of nanofluid only are large at concentrations of 2.5%wt and 5%wt, it is possible that the concentrations are too high for this particle shape. Particle size of the nanofluids was also measured after a month of being made, with only an increase in particle size of 10%. The titania nanofluids, although the particles do settle down to the bottom with time, stay at a consistent particle size, making it a very stable nanofluid.

The viscosity measured of the titania nanofluid at various concentrations are shown in Figures 30, 31, 32, and 33. At first glance, it would seem that most of the nanofluids are shear thickening, but this is not so. With further inspection it can be seen that the results for plain distilled water also appear to be shear thickening, so the only possible explanation for this is that the equipment used is not appropriate for measuring the viscosity of water.

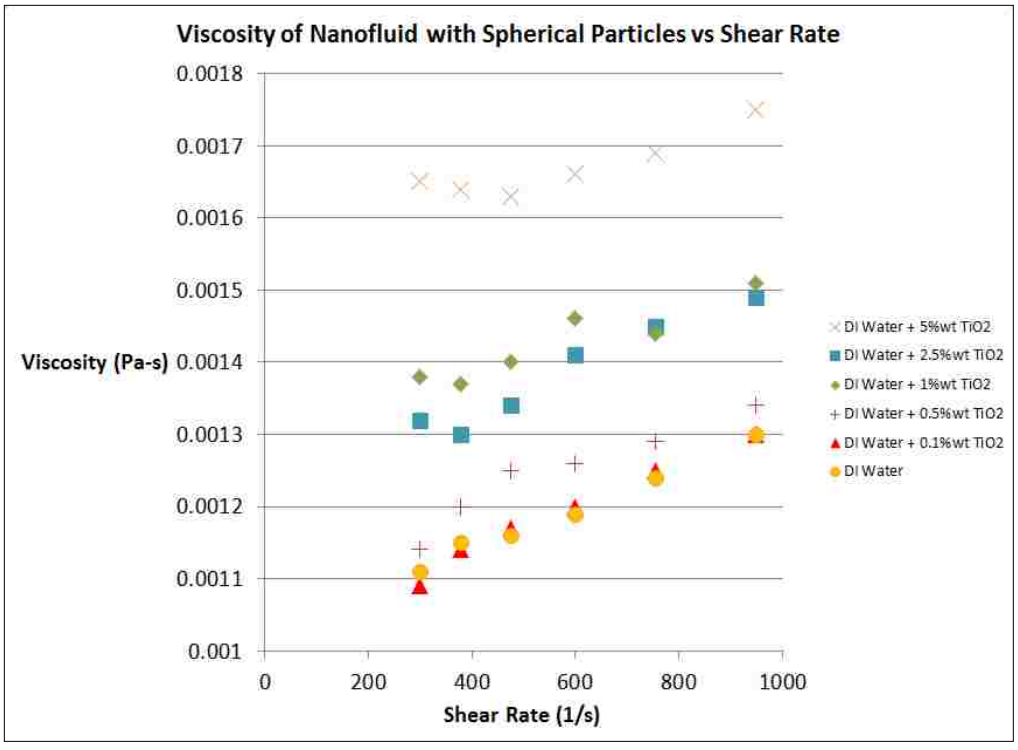

Figure 30: Viscosity of nanofluids with spherical titania nanoparticles at various concentrations vs. shear rate.

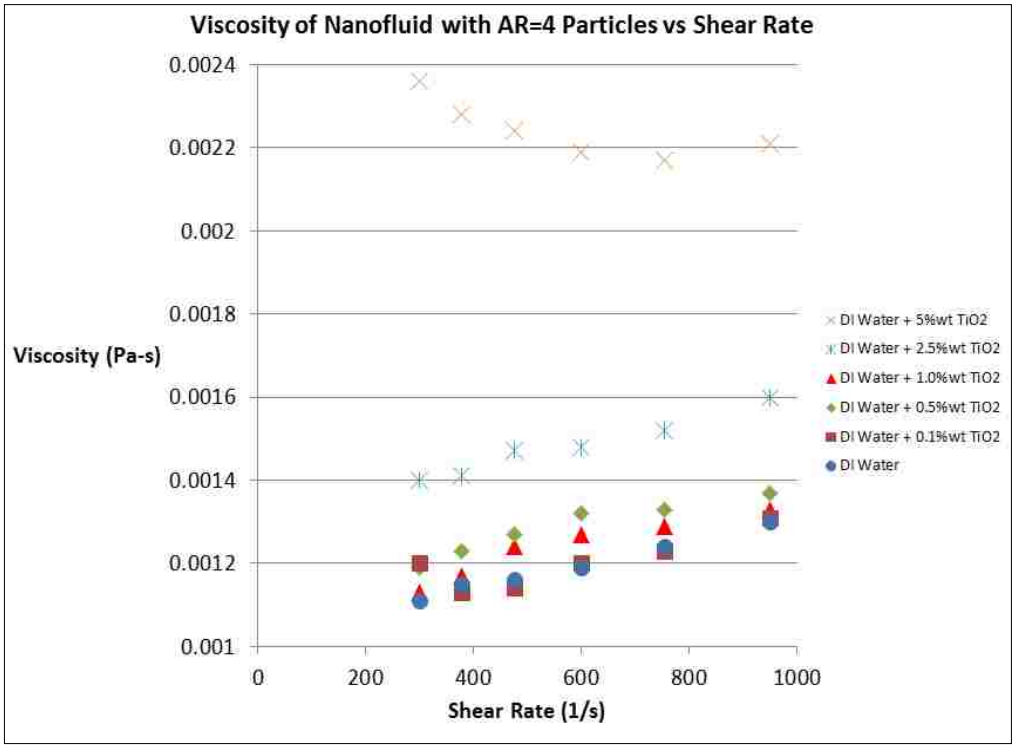

Figure 31: Viscosity of nanofluids with titania nanoparticles of aspect ratio four at various concentrations vs. shear rate.

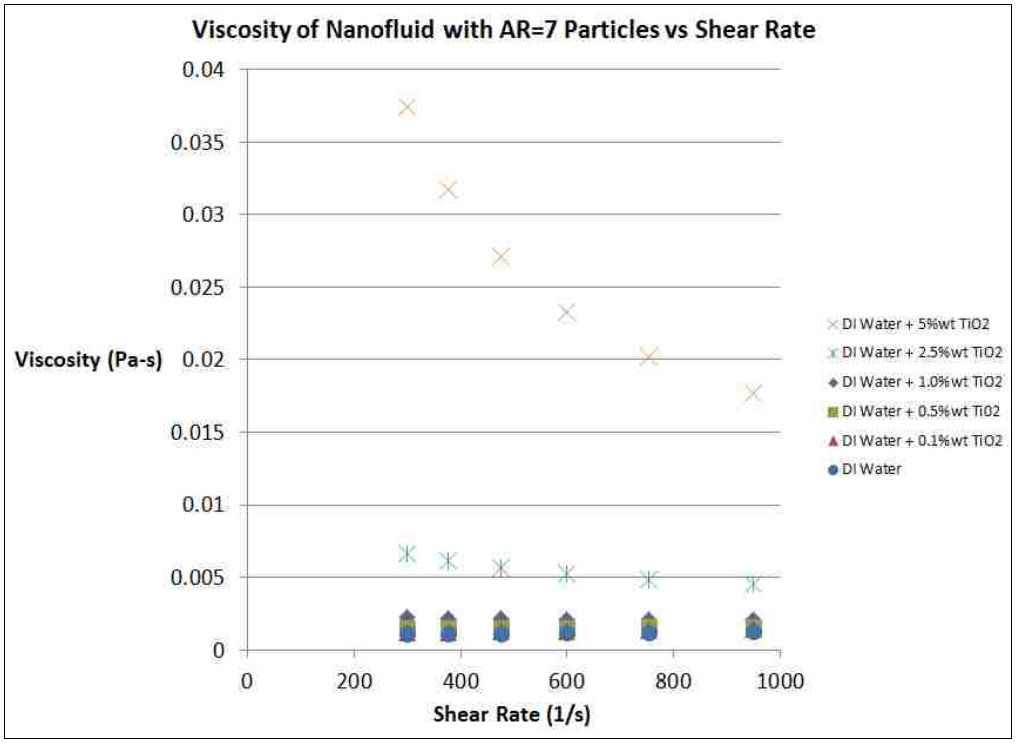

Figure 32: Viscosity of nanofluids with titania nanoparticles of aspect ratio seven at various concentrations vs. shear rate.

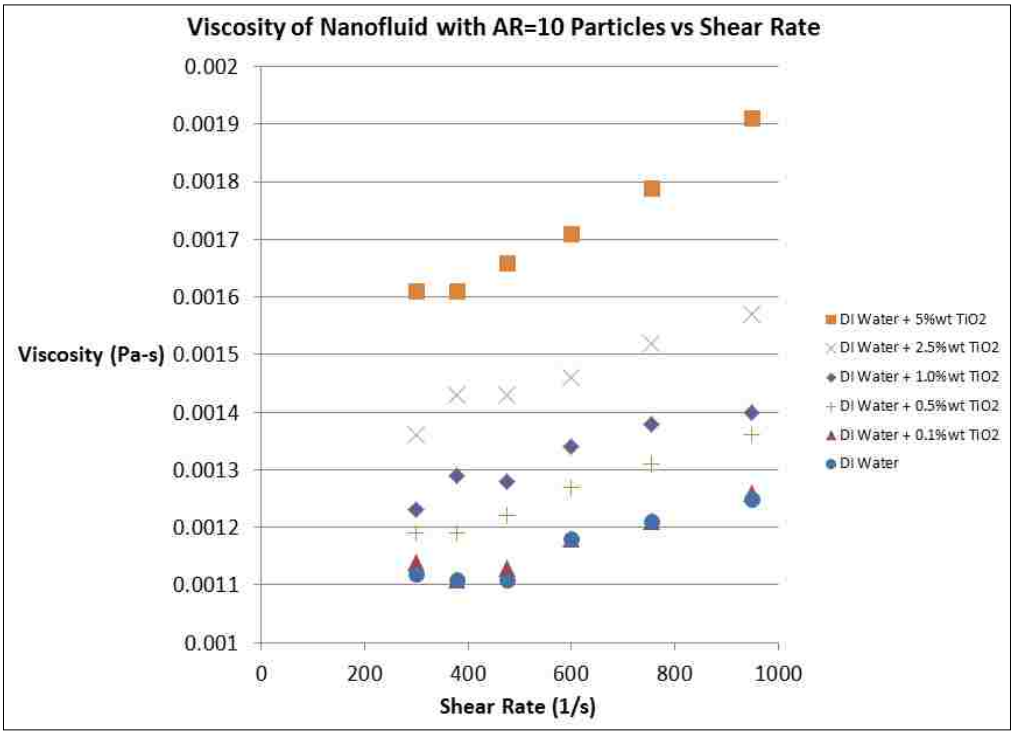

Figure 33: Viscosity of nanofluids with titania nanoparticles of aspect ratio ten at various concentrations vs. shear rate.

For the nanofluid with spherical titania, at all concentrations the viscosity follows the same trend as water, so it is therefore a Newtonian fluid. The viscosity of nanofluids does increase as the concentration of particles increases. When 0.1%wt titania nanoparticles are added there is a negligible change in viscosity. There is a 5% increase in viscosity for 0.5%wt titania nanofluid. When 1%wt titania nanoparticles are added there is a 20% increase in viscosity. A 16% increase in viscosity is observed for 2.5%wt titania nanofluid, while a 40% increase in viscosity is observed for 5%wt titania nanofluid as shown in Figure 30.

For the nanofluid with nanoparticles with an aspect ratio of four, the fluid is Newtonian at concentrations of 0.1%wt, 0.5%wt, 1%wt, and 2.5%wt; however, at a concentration of 5%wt, the fluid is now non-Newtonian and exhibits a shear-thinning effect, as shown in Figure 31. When 0.1%wt titania nanoparticles are added there is again a negligible change in viscosity. When

0.5%wt titania nanoparticles are added there is a 7% increase in viscosity. When 1%wt titania nanoparticles are added there is a 4% increase in viscosity. When 2.5%wt titania nanoparticles are added there is a 24% increase in viscosity.

For the nanofluid with nanoparticles with an aspect ratio of seven, the fluid is Newtonian at concentrations of 0.1%wt, 0.5%wt, and 1%wt; however, at concentrations of 2.5%wt and 5%wt, the fluid is now non-Newtonian and exhibits shear-thinning effects. When 0.1%wt titania nanoparticles are added there is a 10% increase in viscosity. When 0.5%wt titania nanoparticles are added there is a 32% increase in viscosity. When 1%wt titania nanoparticles are added there is a 84% increase in viscosity, as shown in Figure 32.

For the nanofluid with nanoparticles with an aspect ratio of ten, at all concentrations the viscosity follows the same trend as water, so it is therefore a Newtonian fluid. When 0.1%wt titania nanoparticles are added there is a negligible change in viscosity. When 0.5%wt titania nanoparticles are added there is a 8% increase in viscosity. When 1%wt titania nanoparticles are added there is a 13% increase in Viscosity. When 2.5%wt titania nanoparticles are added there is a 25% increase in viscosity. When 5%wt titania nanoparticles are added there is a 47% increase in viscosity, as shown in Figure 33.

As can be seen by the data, the nanofluids with spherical titania and with nanoparticles of aspect ratio ten behave the most similarly. Since the nanofluids with particles of aspect ratio four and seven exhibit shear thinning at higher concentrations, these nanofluids are not optimal for commercial usage. For the spherical and aspect ratio ten nanofluids, at high concentrations there is a significant increase in viscosity which is not ideal and should be addressed before commercial usage.

The thermal conductivity results were very good, contrary to what was expected. The thermal conductivity of the titania nanoparticles alone is 9W/m-K. A graph of the results from the nanoflash device can be seen in Figure 34, while the results from the modified transient plane device can be seen in Figure 35.

\

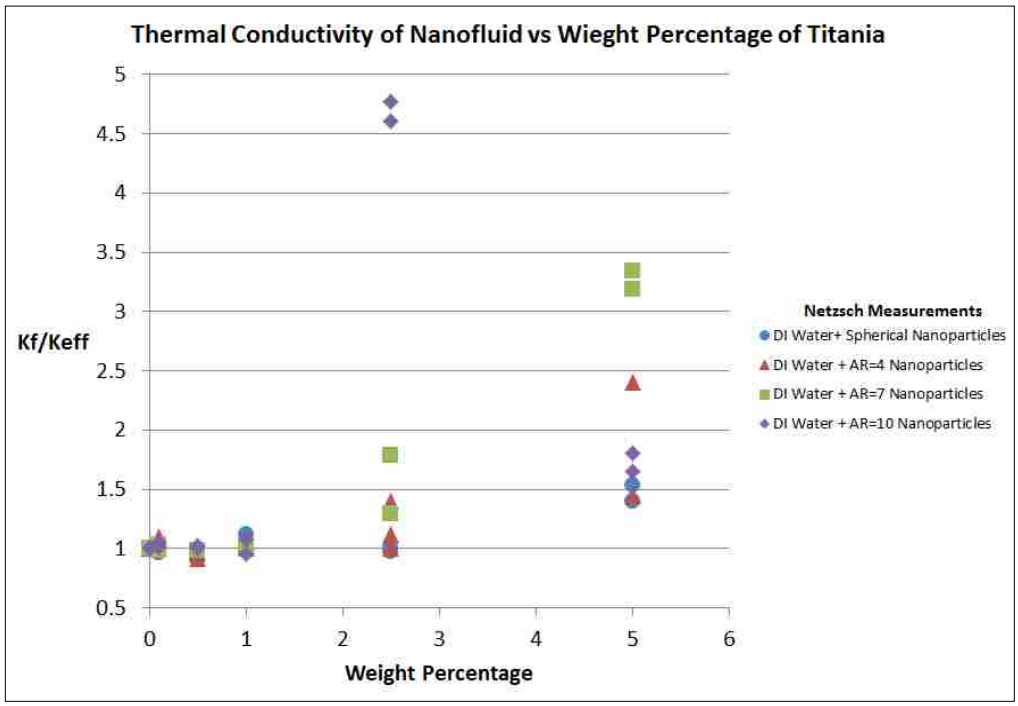

Figure 34: Thermal conductivity measurements collected using a nanoflash device for titania nanofluids at various concentrations.

The modified transient plane results confirm the measurements taken using the nanoflash device and vice versa. From 0.1%wt to 1%wt for all four kinds of titania nanofluids there is less than a 10% increase in the thermal conductivity, which is shown by both the transient plane results and by the nanoflash results. The difference between the transient plane results and the nanoflash results is also less than 10%.

However, as we increase the concentration to 2.5%wt and 5%wt, transient plane results also show less than a 10% increase, as shown in Figure 35. Specifically, at a concentration of

2.5%wt with spherical nanoparticles there is a 2.5% increase in thermal conductivity. When using particles with an aspect ratio of four, at there is a 2.4% increase in thermal conductivity. When using particles with an aspect ratio of seven, there is a 3.2% increase in thermal conductivity. When using particles with an aspect ratio of ten, there is a 7% increase in the thermal conductivity. As can be seen by the data, as the aspect ratio increases, so does the increase in thermal conductivity.

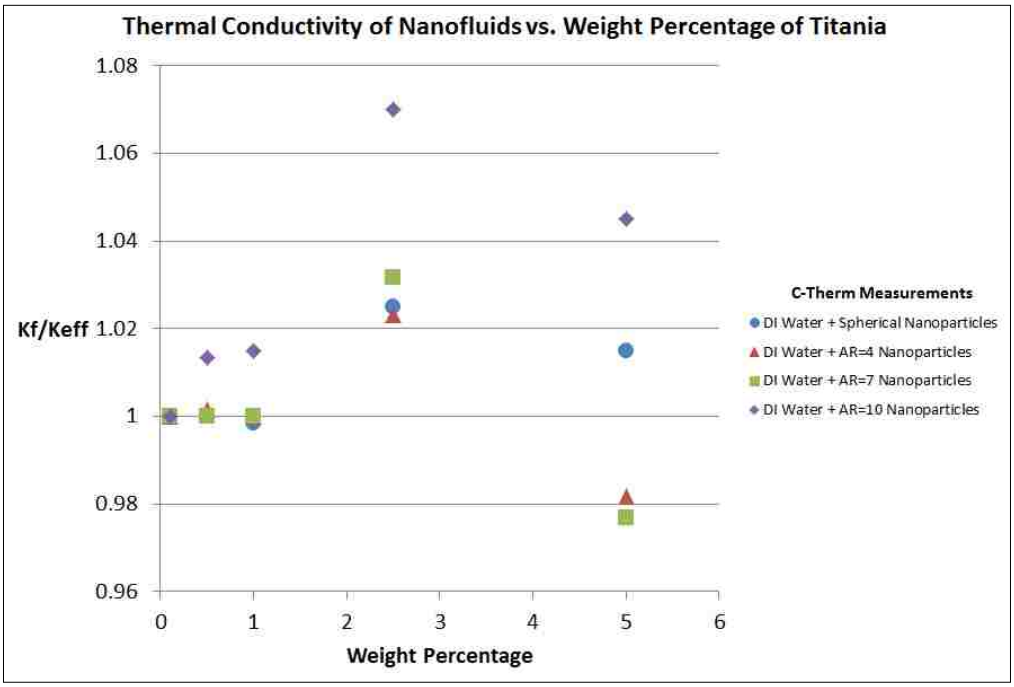

Figure 35: Thermal conductivity measurements collected using transient plane method for titania nanofluids at various concentrations.

When the nanoflash method is used to measure the thermal conductivity of the nanofluids at a 2.5%wt concentration, the results are at times very similar to those of the transient plane results, but at times also very different. When using the spherical nanoparticles, the results are almost exactly the same, with an increase of 2% in the thermal conductivity, very similar to the 2.5% increase shown by the transient plane. When using particles with an aspect ratio of four,

the results are mixed, with an increase of 1% being very close to the 2.4% increase found with the transient plane, yet an increase of 12% was also observed using the nanoflash device. Considering the results, it is more likely that the 1-2.4% increase is the precise one, since it is confirmed using both methods. When examining the results for the nanoparticles of aspect ratio seven, the nanoflash results are radically different from the transient plane ones. The nanoflash results claim an increase of 30-80%, which when compared to the 3.2% found by the transient plane method produce a huge error. When taking into consideration the previous results, it is much more likely that the 3.2% increase is more accurate. Lastly, when examining the results for nanoparticles of aspect ratio ten, there is an enormous difference between the transient plane results and the nanoflash results. The nanoflash results show that the thermal conductivity increases by about 370%, which would be extraordinary if it were accurate; however, when compared once again to the transient plane result of only a 7% increase, it is obvious that one of them must be incorrect.

Moving on to the measurements at a concentration of 5%wt, it can be seen that the similar conclusions apply. The transient plane results show no increase in thermal conductivity until the nanoparticles of aspect ratio ten are used, in which case an increase of about 4% is observed. When examining the results from the nanoflash equipment a much larger increase is observed. With spherical nanoparticles an increase of 40-50% is observed. With nanoparticles of aspect ratio four a 40-140% increase is observed. With nanoparticles of aspect ratio seven a 120-140% increase is observed. With nanoparticles of aspect ratio ten a 65-80% increase is observed. As can be seen, these results are at least one order of magnitude larger than the transient plane results. At this point it is uncertain which results are the correct ones, but one would tend to think that the transient plane ones follow a more consistent trend and must

therefore be the true results. Once again the thermal conductivity tends to increase as the aspect ratio increases.

Chapter 7. Conclusions

Although the particle size results proved to be positive since consistently small sizes were measured, the fluids at high concentrations settled down very quickly, meaning thermal conductivity measurements were very difficult to take at high concentrations, such as 2.5%wt and 5%wt. While the fluid was in the equipment, the particles would settle down and form a layer on the bottom, which acted as a solid rather than as a suspension, which may have caused the thermal conductivity measurements to falsely exhibit extremely large increases. At the same time, this settling phenomenon also happened with the carbon nanoparticles which we tested and it happened to YiJun Yang, a fellow colleague who characterized nanofluids with spherical nanoparticles. In both these sets of data where settling occurred, no increase in thermal conductivity was measured. This leads us to believe that the solid layer theory behind the increase is incorrect. On the other hand, a reason for the low increase in thermal conductivity measured by transient plane method could also be related to the settling. Since the transient plane method requires a sensor to be inserted into the cup, if the nanoparticles have settled to the bottom, the sensor does not come in contact with most of the nanoparticles, and therefore would measure a lower thermal conductivity. Which method is correct cannot be determined until further experiments are performed.

The viscosity measurements show that, unlike the theory that Ding had which states that nanofluids with elongated nanoparticles will exhibit non-Newtonian behavior in the form of shear thinning, our nanofluids only show shear thinning at 5%wt with nanoparticles of aspect ratio four and seven and at 2.5%wt with nanoparticles of aspect ratio seven. However, since there is some uncertainty in exactly how much the thermal conductivity increasesat 2.5%wt and 5%wt concentrations, these gains could be annulled by the increases in viscosity. At 2.5%wt and 5%wt there is a minimum increase in viscosity of 17% and a maximum of 47%, which means

that any energy savings made by the increase in thermal conductivity might not be enough to make up for the increase in viscosity as well. This is especially true if the transient plane results are the true results, since there is only a maximum of 10% increase in thermal conductivity.

Since both experimental methos show increases in thermal conductivity, there must be a physical mechanism causing such increases. A possible explanation that is connected with both the increase in concentration and the increase in aspect ratio is the formation of networks made by the nanorods, which better conduct the applied heat. In essence, these networks act allow for enhanced heat transfer, much like large fins in a duct would.

So in summary, the conclusions brought about by this research are as follows:

- The current method of making titania nanorods is limited in the quantity of titania that can be made.
- Due to the method used to manufacture the titania nanoparticles, the current aspect ratio of the titania nanorods is limited to a maximum of ten.
- Viscosity does increase as more titania nanoparticles are added to water.
- Viscosity can be shear thinning at large concentrations of titania in water.
- Particle size is stable and consistent for the titania nanofluid as long as the titania is never dried. Titania must be kept in the fluid in which it is synthesized, it cannot be dried and then remixed. This would cause a huge increase in particle size.
- The thermal conductivity of titania nanofluids increases as the concentration increases.
- The thermal conductivity of titania nanofluids increases as the aspect ratio increases.

- Synthesis of Al_2O_3 nanotubes is not possible through milling or quenching of membrane discs and other methods should be sought to create alumina nanofluids.
- Stable nanofluids with carbon nanotubes and carbon nanofibers could not be made with methods available to the research project.

Chapter 8. Further Research

Further research into this field should include finding a way to make higher concentration suspensions more stable using both titania nanorods, carbon nanotubes, and carbon nanofibers, which means that surfactants will be explored. With the introduction of surfactants will come the characterization of the nanofluid with surfactant and the effects it has on particle size, viscosity, and thermal conductivity. Also pertinent to nanofluid synthesis is the problem that currently, only small quantities of the titania nanoparticles can be made and the maximum aspect ratio achievable is ten. If larger quantities at equal or larger concentrations are desired, then other methods of titania synthesis must be explored. If larger quantities of the titania nanofluid can be made, then experiments into the heat transfer coefficient should be done. Ulterior methods of titania synthesis should also be sought in order to obtain larger aspect ratios. Also, a more accurate form of measuring the viscosity of water should be sought. Lastly, further research into why transient plane method and nanoflash method produce such different results for thermal conductivity should be done.

Bibliography

1. Choi, S. etc. “Anomalous Thermal Conductivity Enhancements in Nanotube Suspensions.” Applied Physical Letters 79.14 (2001): 2252-2254.

2. Choi, S., etc. “Enhancing Thermal Conductivity of Fluids with Nanoparticles.”

3. Choi, S., etc. “Measuring Thermal Conductivity of Fluids Containing Oxide Nanoparticles.” Journal of Heat Transfer 121.2 (1999): 280-290.

4. Kabelac, S. and Kuhnke, J. “Heat Transfer Mechanisms- Experiments and Theory.” Helmut-Schmidt University of the Federal Armed Forces, Hamburg, Germany.

5. Buongiorno, J., etc. “A Benchmark Study on the Thermal Conductivity of Nanofluids.” Journal of Applied Physics 106.094312 (2009): 1-14.

6. Murshed, S., etc. “Enhanced Thermal Conductivity of TiO_2-Water Based Nanofluids.” International Journal of Thermal Sciences 44 (2005): 367-373.

7. Xie, H., etc. “Thermal Conductivity Enhancement of Suspensions Containing Alumina Particles.” Journal of Applied Physics 91.7(2002).

8. Routbort, J., etc. “Particle Shape Effects on Thermophysical Properties of Alumina Nanofluids.” Journal of Applied Physics 106. 014304 (2009): 1-10.

9. Routbort, J., etc. “Application of SAXS to the Study of Particle Size Dependent Thermal Conducticity in Silica Nanofluids.” Journal of Nanoparticle Research 10 (2008): 1109-1114.

10. Yu, W., etc. “The role of Interfacial Layers in the Enhanced Thermal Conductivity of Nanofluids: a Renovated Maxwell Model.” Journal of Nanoparticle Research 5 (2003): 167-171

11. Xuan, Y., etc. “Aggregation Structure and Thermal Conductivity of Nanofluids.” AlChE Journal 49.4 (2003): 1038-1043.

12. Peterson, G., etc. “The Effect of Particle Size on the Effective Thermal Conductivity of Al_2O_3-Water Nanofluids.” Journal of Applied Physics 101.4 (2007).

13. Wang, B., etc. “A Fractal Model for Predicting the Effective Thermal Conductivity of Liquid with Suspension of Nanoparticles.” International Journal of Heat and Mass Transfer 46 (2003): 2665-2672.

14. Routbort, J., etc. “Pumping Power of Nanofluids in a Flowing System.” Journal of Nanoparticle Research (2011).

15. Ding, Y., etc. “Relationship Between the Thermal Conductivity and Shear Viscosity of Nanofluids.” Physica Scripta T139 (2010): 1-7.

16. Kwak, K and Kim, C. “Viscosity and Thermal Conductivity of Copper Oxide Nanofluid Dispersed in Ethylene Glycol.” Korea-Australia Rheological Journal 17 (2005)::35-40.

17. Prasher, R., etc. “Brownian Motion Based Convective-Conductive Model for the Effective Thermal Conductivity of Nanofluids.” Journal of Heat Transfer 128 (2006): 588-595.

18. Praveen K, etc. “Viscosity of Copper Oxide Nanoparticles Dispersed in Ethylene Glycol and Water Mixture.” Exp. Therm. Fluid Science 32 (2007) 397-402.

19. Tsai T, etc. “Effect of Viscosity of Base Fluid on Thermal Conductivity of Nanofluids.” Applied Physics Letters 93.23 (2008).

20. Zhang Q and Gao L. “ Preparation of Oxide Nanocrystals with Tunable Morphologies by the Moderate Hydrothermal Method: Insights from Rutile TiO_2.” Langmuir 19 (2003): 967-971.

Vita

Valentina Baio daughter of Michael and Vanda Baio was born on July 12, 1987 near Philadelphia, PA. Her preliminary education was in Philadelphia, with summers and Christmas holidays in Palermo, Italy where their family is from. She completed a B.S. degree in Mechanical Engineering at Lehigh University in 2009 and is currently submitting this thesis for an M.S. degree